Available online at www.sciencedirect.com
ScienceDirect
Trans. Nonferrous Met. Soc. China 32(2022) 2770−2786
Transactions of Nonferrous Metals Society of China
www.tnmsc.cn

Adsorption of lead ions by a kind of MAL modified hydrogel beads

Chun-li ZHENG[1,2*], Qiao-rui WANG[1*], Guo-qing GENG[3], Zhen-xing WANG[4], Heng ZHUO[5]

1. Department of Environmental Science and Engineering, Xi'an Jiaotong University, Xi'an 710049, China;
2. Key Laboratory of Subsurface Hydrology and Ecological Effect in Arid Region of Ministry of Education, Chang'an University, Xi'an 710049, China;
3. Department of Civil and Environmental Engineering, National University of Singapore, 117576, Singapore;
4. South China Institute of Environmental Sciences, Ministry of Ecology and Environment (MEE), Guangzhou 510655, China;
5. Jiangsu TST Professional Testing Co., Ltd., Suqian 223800, China

Received 28 July 2021; accepted 17 February 2022

Abstract: Hydrogel-I was fabricated via sodium alginate in situ-embedding with MAL powders and then applied to decontaminating Pb(II) from water. Conditions for preparing Hydrogel-I and the adsorption of Pb(II) over Hydrogel-I were optimized through response surface methodology coupled with central composite design. XPS revealed that the groups of —OH, —COO—, —NH, —NH_2 and —CSS— carried by Hydrogel-I were responsible for the uptake of Pb(II). Ions exchange, surface complexation, electrostatic attraction and pore-filling effect contributed to the adsorption process. Adsorption performances of Pb(II) by Hydrogel-I and MAL powders were compared. Although they exhibited similar adsorption rate and maximum adsorption capacity (q_m), the reusing ability of Hydrogel-I was better and it was easier to be separated from aqueous solution after treatment. Even compared with organic hydrogel materials, Hydrogel-I presented relatively quick adsorption speed and high adsorption capacity. It can be concluded that Hydrogel-I could be an alternative scavenger for the treatment of Pb(II) from aqueous solution.
Key words: adsorption; MAL powder; hydrogel bead; Pb(II)

1 Introduction

Lead(II) is commonly regarded as the most poisonous heavy metal due to its degradation-resistance, bio-accumulation and high toxicity [1]. Several processing techniques are adopted for purifying the contamination of Pb(II) including chemical extraction separation [2], electrochemical osmosis [3], adsorption [4] and phytoremediation [5]. Among them, adsorption for metal ions from wastewater or water by solid scavengers has aroused the interest of researchers attributing to its characteristics of design flexibility, high reliability, convenient recyclability and easy operation [6]. As for solid adsorbents, lignin belongs to bio-polymer and possesses a wide range of sources, which draws significant attention as the groups of phenolic/alcoholic hydroxyl (—OH), carbonyl (C═O) and methoxyl (—OCH_3) do [7]. However, the removal ability of lignin for heavy metals is low [8] so that introducing the additional functional groups on lignin skeleton is necessary. In our previous studies, two reagents of polyethyleneimine (PEI) and carbon disulfide (CS_2) were used for co-modifying alkaline lignin (AL) to prepare scavenger of MAL (Table S1 in Supporting information) powders accompanied by the functional groups of imine (—NH), amine (—NH_2) and dithiocarbamate (—CSS—) grafted [9]. The maximal adsorption

* Chun-li ZHENG and Qiao-rui WANG contributed equally to this work
Corresponding author: Zhen-xing WANG, Tel/Fax: +86-20-85525941, E-mail: wangzhenxing@scies.org
DOI: 10.1016/S1003-6326(22)65983-1

capacity (q_m) of MAL towards Pb(II) was calculated to be 79.9 mg/g [9], showing an adsorption advantage compared to raw lignin of 8.9 mg/g [10]. As MAL is powder in nature, the disadvantage of MAL is that it is difficult to be separated from aqueous solutions after treatment. This disadvantage might result in material waste and secondary pollution.

Hydrogel spheres possess such features as suitable size, porosity, facile operation and easy separation, and can be considered to be the prospective adsorbents [11]. Sodium alginate (SA) from algae is classified into a type of natural polysaccharide [12]. Since SA carries abundant functional groups of hydroxyl (—OH) and carboxyl (—COOH), it can immobilize environmentally-friendly and cost-effective hybrid composites into insoluble hydrogel through ionotropic gelation [13]. For instance, several researches focused on fabricating hydrogels of polyacrylamide-graphene oxide-sodium alginate (SA-PAM/GO) [14], carboxylated cellulose nanocrystal-sodium alginate (CCN-Alg) [15] and bentonite-carboxymethyl chitosan-sodium alginate (Mag-Ben/CCS/Alg) [16] by embedding polyacrylamide/graphene oxide [14], carboxylated cellulose nanocrystal [15] and magnetic bentonite/carboxymethyl chitosan [16] into the calcium-alginate beads, respectively. These hydrogel beads were used for the decontamination of heavy metals from aqueous solution, in which the maximum adsorption capacity (q_m) of Pb(II)/Cu(II), Pb(II) and Cu(II) was 240.7/68.8, 338.9 and 56.8 mg/g over SA-PAM/GO [14], CCN-Alg [15] and Mag-Ben/CCD/Alg [16] correspondingly, demonstrating good adsorption performance. Furthermore, the regeneration ability for the aforementioned hydrogel beads also proved to be ideal [14−16]. However, deep investigations including adsorption mechanisms for heavy metals still need to be further explored. Besides, although powder adsorbents embedded into SA hydrogels could improve their separation performances, different synthesizing conditions for hydrogels could result in different adsorption abilities. Therefore, conditions in the synthesis process were required to be optimized.

This work focused on preparing a kind of hydrogel embed with PEI and CS_2 co-modified lignin (MAL), in which SA was used as matrix mixed with MAL powders. Calcium chloride ($CaCl_2$) solution was used to be the cross-link agent. The optimal conditions for preparing hydrogel beads and adsorbing Pb(II) were determined. The adsorption mechanism was revealed and the adsorption performance was evaluated. The separation and regeneration performances of hydrogel beads were conducted. This work also aims at providing a kind of material which has an application potential for the treatment of Pb(II)-loaded wastewater or water.

2 Experimental

2.1 Chemicals

The analytical reagents of AL and SA were obtained from Anhui Zhonghong Biological Engineering Co. Ltd. (Anhui, China). The branched PEI (M_w=70000, ca. 30% in water) was supplied by Sigma-Aldrich (Shanghai) Trading Co. Ltd. Other reagents including calcium chloride ($CaCl_2$), hydrochloric acid (HCl), formaldehyde (HCHO), sodium hydroxide (NaOH) and CS_2 were all provided from Shanghai Hongrui Chemical Co., Ltd. (Shanghai, China). The standard solution of lead nitrate (Pb(II), 1000 mg/L) was brought from Beijing Beina Chuanglian Biotechnology Research Co. Ltd. (Beijing, China). Ultrapure water was applied throughout the experiments and prepared by using UPR-II-10TNZ equipment (Zhengzhou Youerpu Instrument Equipment Co. Ltd., Henan, China).

2.2 Determination of optimal condition for preparing hydrogel beads

The modified AL, named as MAL, was synthesized by ourselves. Its preparation and characterization have been described in our previous report [9]. Text S1 in the Supporting information (SI) described MAL detailedly. The optimal conditions for preparing hydrogel beads were given in Text S2 (SI), in which MAL powders was mixed with SA solution and then generated gelation in the presence of $CaCl_2$ solution. Significant variables for Hydrogel-I preparation were selected using method of response surface methodology coupled with plackett-burman (RSM-PB). Minimum run resolution V design of Design expert 8.0.6 software was employed for

screening significant variables with keeping the removal efficiency (%) of Pb(II) (C_0=10 mg/L) as a response variable. Five independent variables including initiator composition (SA, wt.%, *A*), crosslinker concentration ($CaCl_2$, mol/L, *B*), beads diameter (mm, *C*), reaction time (min, *D*) and powder amount (MAL, g, *E*) corresponded to 2.0 or 4.0 wt.%, 0.1 or 0.3 mol/L, 3.0 or 6.0 mm, 30 or 720 min and 0.1 or 0.4 g were considered into RSM-PB design. Twelve experiments were carried out, as given in Table S2. Analysis of variations (ANOVA) (p<0.0500) could validate the factorial model and provide a simplified model by removing non-significant terms.

To determine the optimal conditions for preparing hydrogel-beads, the method of response surface methodology coupled with central composite design (RSM-CCD) was adopted. Three independent variables of initiator composition (SA, wt.%, *A*), crosslinker concentration ($CaCl_2$, mol/L, *B*) and powder amount (MAL, g, *E*) corresponded to 2.0, 3.0 and 4.0 wt.%, 0.1, 0.2 and 0.3 mol/L and 0.1000, 0.2000 and 0.4000 g were further selected based on the results of RSM-PB design (Table S3). These three independent parameters were designed with 3 coded values (−1, 0 and +1) through twenty experiments (Table S4). The detailed descriptions for these steps can be seen in Text S2 (SI).

2.3 Characterizations of hydrogel beads

The as-prepared hydrogel beads were named Hydrogel-I. Physicochemical properties of Hydrogel-I were tested using Fourier transform infrared spectroscopy (FT-IR), zeta potential, thermogravimetric analysis (TGA), derivative thermogravimetric (DTG), scanning electron microscope (SEM) combined with the dispersive spectroscopy (EDS), N_2 adsorption−desorption isotherm, compressive strength measurement and X-ray photoelectron spectroscopy (XPS). Text S3 in SI presents the detailed steps for the afore-mentioned measurements.

2.4 Adsorption tests

Adsorption tests in this work included determination of the optimal condition for the adsorption of Pb(II), adsorption isotherm, adsorption kinetics, adsorption thermodynamics, and regeneration. The detailed descriptions are exhibited in Text S4 and Text S5 (SI).

2.5 Analysis

The residual concentrations of Pb(II) were analyzed by using inductively coupled plasma optical emission spectrometry (ICP-OES) (Thermo, USA).

3 Results and discussion

3.1 Optimization of Hydrogel-I preparation

Five process variables of initiator composition (SA, wt.%, *A*), crosslinker concentration ($CaCl_2$, mol/L, *B*), beads diameter (mm, *C*), reaction time (min, *D*) and powder amount (MAL, g, *E*) for Hydrogel-I were considered. A total number of 12 randomized experiments were carried out and the results were presented in Table S2. According to Figs. 1(a, b), half normal plot and Pareto chart display that *A*, *B* and *E* were the most significant variables which affected the removal efficiency of Pb(II). The analysis of variance (ANOVA) for the selected factorial model was presented in Table S3. It can be seen that the values of *F* and *p* were 23.10 and 0.0129 (<0.0500), respectively, suggesting that the model was significant. Moreover, the terms of *A*, *B*, *E*, *AB*, *AE* and *DE* were determined to be significant as p<0.0500 (Table S3). So, the significant variables of *A*, *B* and *E* were selected to be further verified and optimized through the central composite design (CCD), in which a total number of 20 randomized experiments were designed and the according results are listed in Table S4. It was noted here that the values of beads diameter and reaction time (non-significant variables) were fixed at ~3 mm and 0.5 h, respectively. The equation of multiple regression for the actual factors from CCD through Design expert 8.0.6 software by analyzing the experimental data (Table S4) is given as follows:

$$R=85.6-3.2A-5.9B+0.2E+2.4AB-1.1AE+0.5BE-2.5A^2-3.4B^2-0.6E^2 \quad (1)$$

where *R* is the removal efficiency (%).

Table S5 presents the data of ANOVA analysis, in which *F* and *p* values were found to be 16.8 and <0.0001 (<0.0500), respectively, replying that Eq. (1) was significant. The process variables of *A*, *B*, *AB* and B^2 were significant terms because their *p* values <0.050 (Table S5). According to Eq. (1), the maximum removal efficiency of Pb(II) was calculated to be 94% under the conditions of

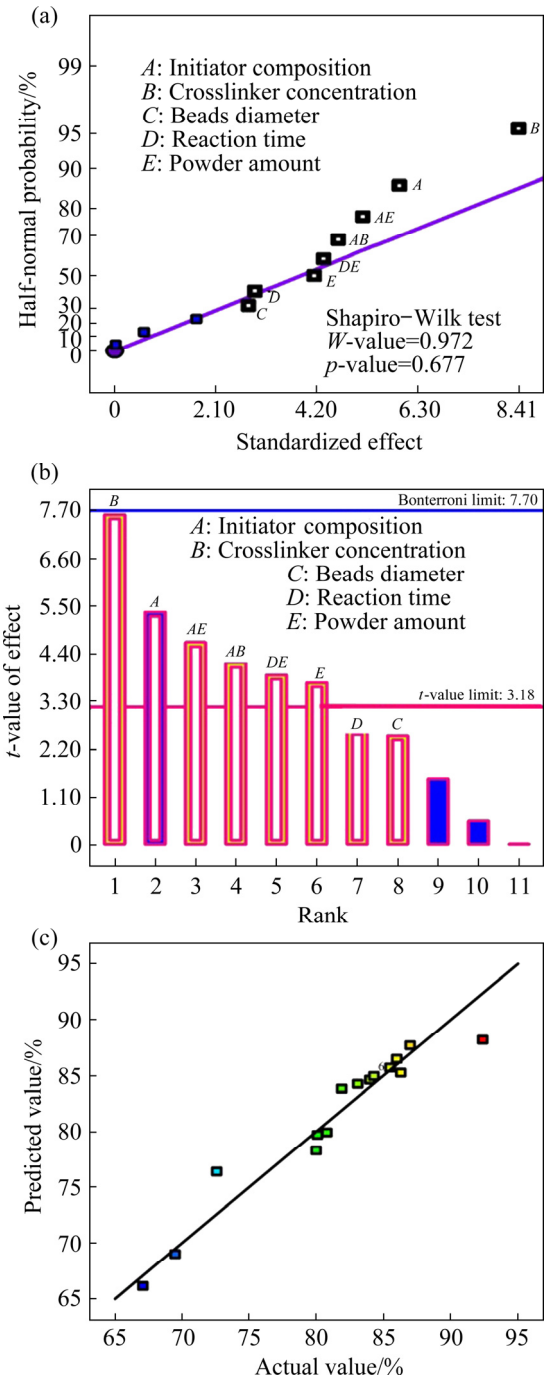

Fig. 1 Half-normal plot (a), Pareto chart (b) and predicted data versus experimental data (c)

initiator composition (A) of 1.20 wt.%, crosslinker concentration (B) of 0.23 mol/L and powder amount (E) of 0.3400 g. When the optimized conditions were used to fabricate Hydrogel-I, the actual removal efficiency of Pb(II) was 92%. These results further confirmed that Eq.(1) was reliable and credible. The correlation coefficient (R^2) of Eq. (1) was 0.9380, demonstrating a good fit between the predicted values of the model and the actual values of experiments (Fig. 1(c) and Table S5). Furthermore, the p value of lack-of-fit was 0.1827 (>0.0500), demonstrating that the lack of fit was not significant.

The response surface plots for the removal efficiency of Pb(II) over Hydrogel-I are exhibited in Fig. 2. The contour maps derived from the response

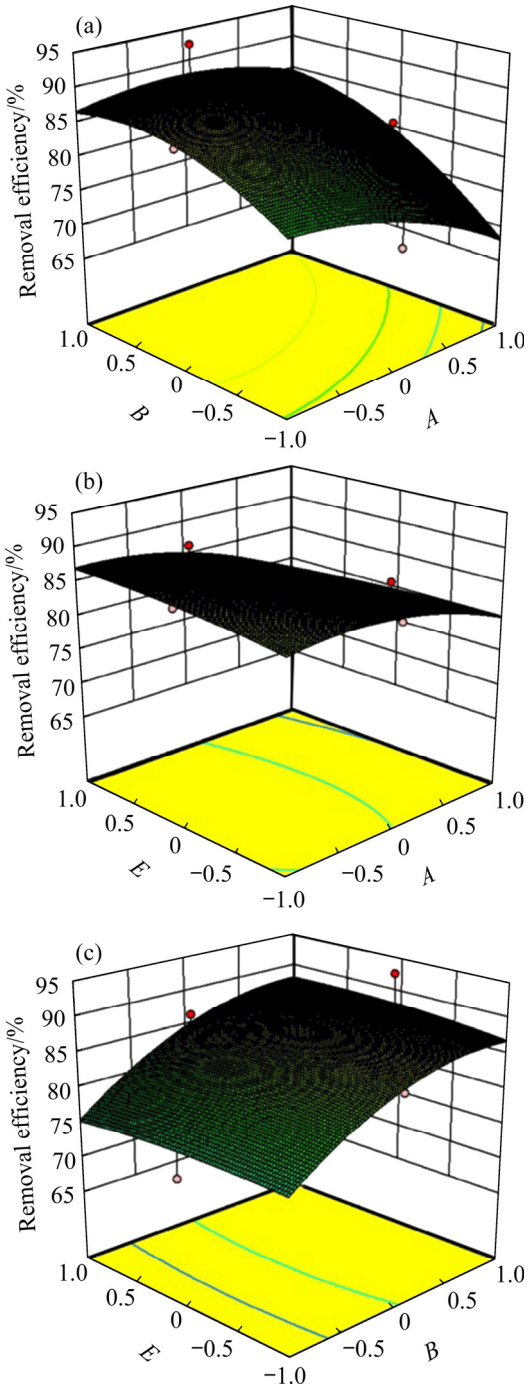

Fig. 2 Response surface plots of initiator composition and crosslinker concentration (a), initiator composition and powder amount (b), and crosslinker concentration and powder amount (c)

surface plots (Figs. 2(a−c)) are presented in Fig. S1. The data of ANOVA analysis (Table S5) showed the interaction of initiator composition (*A*) and crosslinker concentration (*B*) significantly influenced the removal efficiency of Pb(II) since *p*-value of *AB* was 0.0092 (<0.0500). The reason was that the primary skeleton structure of Hydrogel-I was formed through SA and Ca^{2+} ions via crosslinking, as displayed in Scheme 1. When the initiator composition was fixed, the removal efficiency of Pb(II) increased with the increase in crosslinker concentration (Fig. 2(a) and Fig. S1(a)). This phenomenon could be ascribed to the fact that the gel degree was gradually enhanced when the concentration of Ca^{2+} ions was increased, resulting in the densification of gel structure and improving the absorption rate of Pb(II)-loaded aqueous solution [17]. When the crosslinker concentration was fixed, the removal efficiency decreased with the increase in the initiator composition (Fig. 2(a) and Fig. S1(a)). The possible reason was attributed to the occurrence of inadequate crosslinking. The lower ratio of Ca^{2+} ions versus SA could lead to weaker coagulation ability and thinner cortex, which was not conducive to adsorption of Pb(II) onto Hydrogel-I [18]. It was observed that no interaction between powder amount and initiator composition or crosslinker concentration and powder amount (Figs. 2(b, c), Figs. S1(b, c) and Table S5). This was due to MAL powders being just in-situ embedded into Hydrogel-I structure (Scheme 1).

3.2 Characterizations of Hydrogel-I

The photograph of Hydrogel-I is shown in the insert of Fig. 3(a). Its outlook was spherical in shape with diameter of approximately 3 mm. According to the SEM image (Fig. 3(a)), the surface of Hydrogel-I was roughened by particles with diameter of 2−12 μm. On the fracture surface of the bead (Fig. 3(b)), pores ranging from 50 to 70 μm were observed. SEM−EDS demonstrated the existence of Ca element (insert in Fig. 3(a)) since $CaCl_2$ was used as the crosslinker during the preparation process of Hydrogel-I. According to N_2 adsorption−desorption isotherm (Fig. S2(a)), the curves for adsorption and desorption belong to Type III [14], suggesting the existence of porous structure in Hydrogel-I. This result was consistent with SEM analysis. Moreover, the primary porous structure in Hydrogel-I was found to be micro-porous and mesoporous with distribution ratios of 42% (Fig. S2(b)) and 57.5% (Fig. S2(b)), respectively. The average pore size and BET specific surface area of Hydrogel-I corresponded to 2.791 nm (Fig. S2(b)) and 3.371 m^2/g (Fig. S2(a)).

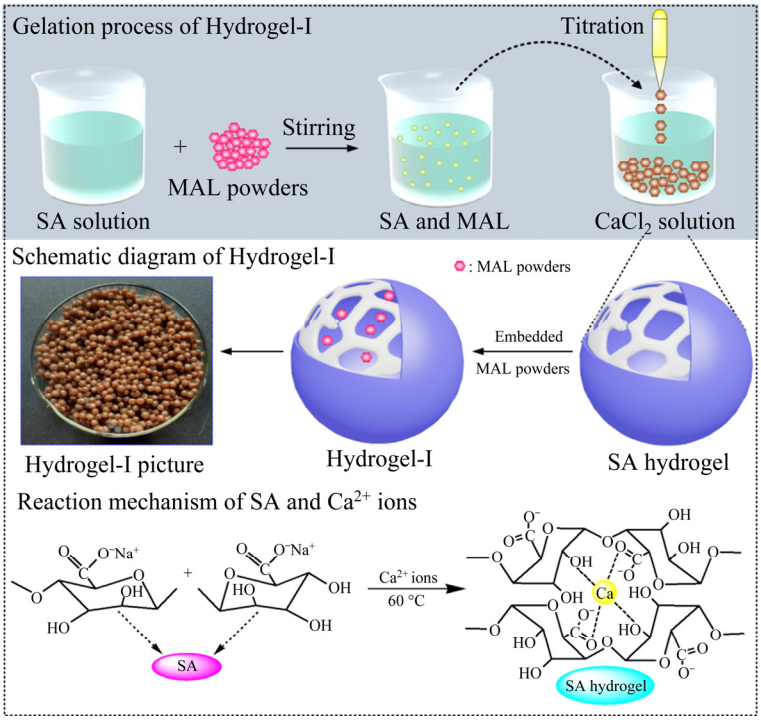

Scheme 1 Schematic diagram of Hydrogel-I

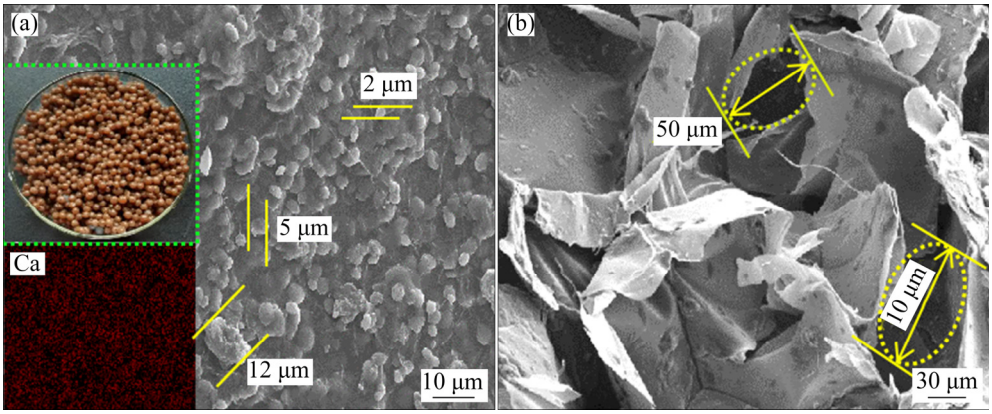

Fig. 3 SEM images of surface structure (inserts are Hydrogel-I picture and EDS of Ca) (a) and internal structure with splitting beads into two pieces (b)

These features of high specific surface area and rich porosity could improve the adsorption of Pb(II) over Hydrogel-I beads.

FT-IR and XPS were used to characterize the functional groups carried by Hydrogel-I. According to Fig. 4, a broad band observed at 3460 cm^{-1} could be assigned to the stretching vibration of —OH [19,20]. The four peaks detected at 1720, 1613, 1418 and 1031 cm^{-1} were attributed to stretching vibration of asymmetric —COO— [21], symmetric —COO— [21], C—OH [22] and C═O [22], respectively. Figure 5(a) shows that the full scan survey XPS spectrum for Hydrogel-I included S 2p, C 1s, N 1s and O 1s. As seen from Fig. 5(b), the spectrum for O 1s by XPS analysis was discovered at 531.02, 53 2.39 and 532.47 eV corresponding to —OH [23], C═O [23] and C—O—(C,H) [23]. Oxygen-containing groups of Hydrogel-I derived from SA since SA was used as the initiator [22]. Figure 4 exhibits that three peaks centered at 1598, 1080 and 856 cm^{-1} belonged to the stretching vibrations of —NH_2 [24], C═S [24] and the deformation vibration of —CSS— [24], respectively. From the spectra of N 1s (Fig. 5(c)) and S 2p (Fig. 5(d)), the existence of —NH (397.89 eV) [23], —NH_2 (399.49 eV) and C—N (401.46 eV) [23], C—S (169.07 eV) [25,26] and C═S (170.23 eV) [25,27] in Hydrogel-I was detected. It was MAL that contributed to the introduction of nitrogen- and sulfur-containing groups on the surface of Hydrogel-I. To evaluate the thermal tolerance of Hydrogel-I, the temperature−mass relation was investigated via thermogravimetric analysis (TGA) coupled to its derivative (DTG)

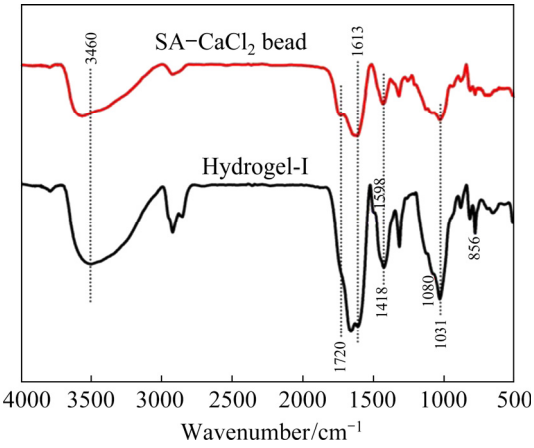

Fig. 4 FT-IR spectra

(Fig. 6). TGA curve exhibited three mass loss stages including water loss stage (20−195 °C), fast degradation stage (195−500 °C) and slow degradation stage (500−800 °C). In the water loss stage (20−195 °C), the mass loss was 12.5%, owing to the loss of the adsorbed water [28]. The mass loss rate was obtained as 0.125%/°C at 98 °C on the basis of DTG curve. A major transformation was discovered in the fast degradation stage (195−500 °C), in which the obvious mass loss was 47.2%. According to DTG curve, the mass loss rate ascended to the maximum value of 0.304 %/°C at lower temperature of 221 °C. The reason was that SA decomposed when the temperature ranged from 200 to 300 °C [28]. Emergence of a shoulder peak indicated that the pyrolysis of SA was not a sole chemical process [29]. The mass loss rate of 0.117 %/°C at higher temperature of 470 °C was attributed to lignin pyrolysis [29]. Due to abundant aromatic rings with various branches, higher

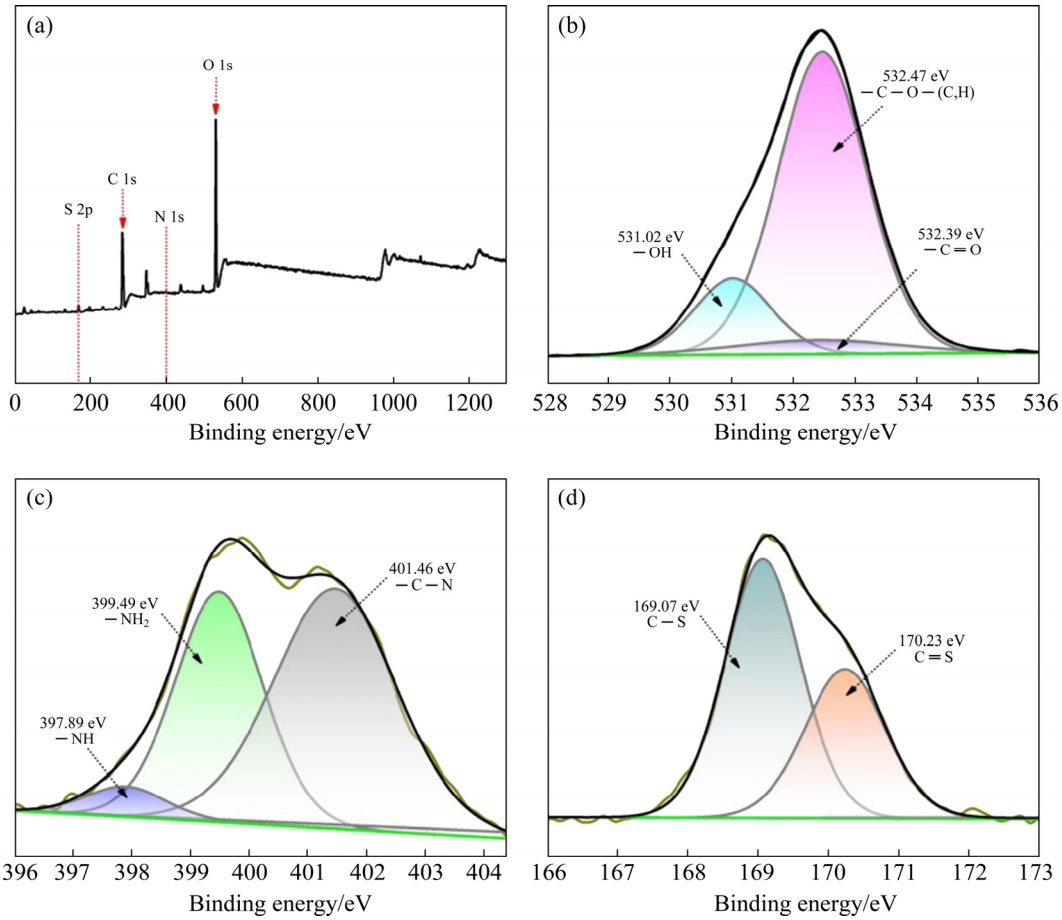

Fig. 5 Full scan survey XPS spectra of Hydrogel-I (a); high resolution spectra of O 1s (b), N 1s (c) and S 2p (d)

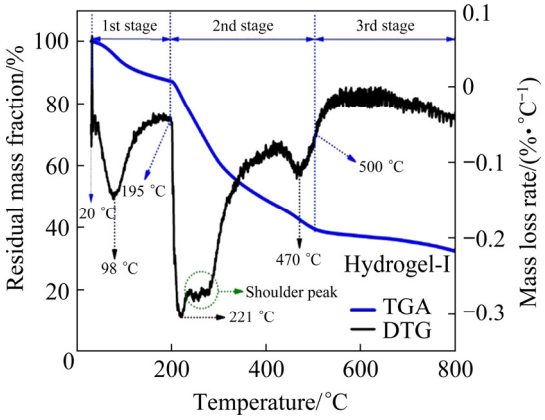

Fig. 6 TGA/DTG curves of Hydrogel-I

temperature was needed for lignin decomposition. As for the slow degradation stage (500−800 °C), the mass loss was found to be 7.1%. Interestingly, the residual mass fraction was 33.2%, higher than the sodium alginate-based beads (SA/PAMPS10) (~20%) [28] and polyacrylic acid modified sodium alginate-based hydrogel (SA-cl-PAA) (~5%) [30]. The higher residual mass fraction of Hydrogel-I was possibly due to the existence of MAL, in which the highly condensed aromatic structure of MAL made it convert to char [29]. As the main thermal degradation occurred at 200−300 and 470 °C, it was demonstrated that Hydrogel-I has a relatively good thermostability.

The compressive property of Hydrogel-I can be seen from Fig. 7. The more detailed calculations for stress (σ) and strain (ε) are given in Text S3 (SI). As shown in Fig. 7, it was observed that σ increased when ε ranged from 0 to 96%, revealing that the energy dissipation inside the network resisted the external force [31]. Corresponded to ε value of 96%, the stress of Hydrogel-I was 6.7 MPa. The elastic modulus (E) of Hydrogel-I was 6.97 MPa, which was higher than that of graphene oxide/sodium alginate hydrogel (0.202 MPa) [22], sodium alginate/polyacrylamide hydrogel (0.81 MPa) [31], chitosan/polyacrylamide double-network hydrogel (0.34 MPa) [32] and cellulose poly(2-hydroxyethyl methacrylate hydrogel (1.25 MPa) [33]. The good mechanical strength of Hydrogel-I might be ascribed to the chains of Ca^{2+} crosslinked with SA [21] and

the addition of MAL [21,31]. These results suggested that Hydrogel-I has a relatively good mechanical strength. Figure 8 also exhibits that pH_{pzc} value of Hydrogel-I was 1.9 based on zeta potential measurement.

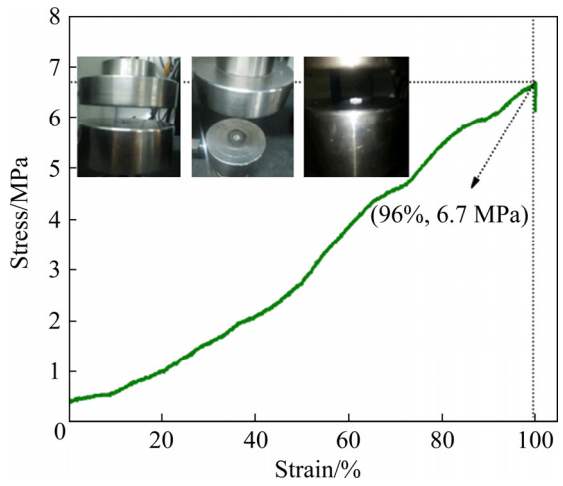

Fig. 7 Compressive strength of Hydrogel-I

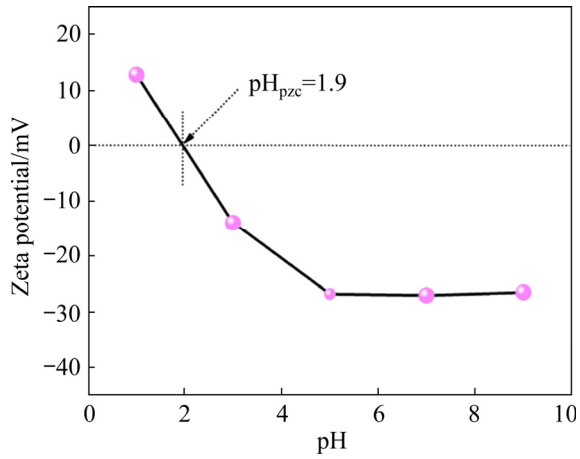

Fig. 8 Zeta potential of Hydrogel-I

3.3 Optimization of Pb(II) adsorption

The influence of independent variables including adsorbent dosage (A), contact time (B) and solution pH (C) on the removal efficiency of Pb(II) was studied through CCD optimization method. A total of 20 batch experiments were performed and the data was fitted through the empirical second-order polynomial. The obtained results are displayed in Table S6. The equation in terms of regression coefficient for Pb(II) adsorption onto Hydrogel-I is exhibited in Eq. (2):

$$R=94.1+10.4A+23.1B+13.2C+1.1AB-4.1AC+10.7BC-1.0A^2-25.4B^2-18.7C^2 \quad (2)$$

The p value was less than 0.0001 (Table S7), indicating that Eq. (2) was significant. The value of p less than 0.0500 revealed that the terms such as A, B, C, BC, B^2 and C^2 were significant. According to Eq. (2), the optimal conditions of adsorbent dosage, contact time and solution pH were performed to be 3.0 g/L, 13 min and 6.0, respectively. The experimental value for the removal efficiency of Pb(II) was 94.9% which was close to the value calculated by Eq. (2) (98.2%). The coefficient of determination (R^2) of Eq. (2) was 0.9614, suggesting a good fit between the predicted values of the model and the actual values from the experiments (Fig. 9 and Table S7). Furthermore, the p value for lack-of-fit was calculated to be 0.1120 (>0.0500), conforming that the lack-of-fit was not significant. These results suggested that Eq. (2) was credible and reliable.

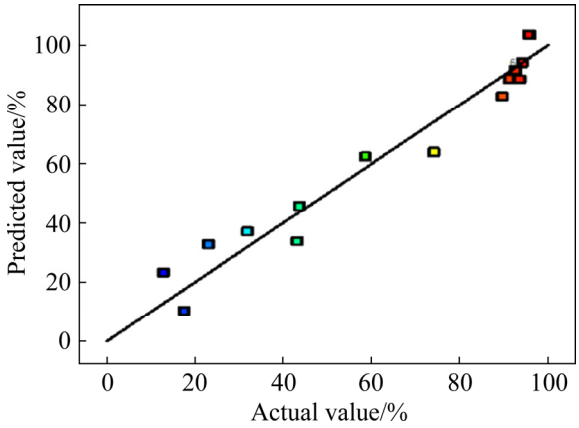

Fig. 9 Predicted data versus experimental data

Table S7 shows there was no interaction relationship between contact time and adsorbent dosage as p-value of AB was 0.7135 (>0.0500). Similar description can be used for adsorbent dosage and solution pH since the p-value of AC was 0.1958 (>0.0500). However, the p-value of BC was observed to be 0.0045, which was lower than 0.0500, suggesting that contact time and solution pH were independent. The response surface plots (Fig. 10) and contour maps (Fig. 11) proved the interaction relationship between contact time and solution pH. The possible reason was that enough contact time ensured relatively complete adsorption reaction between Pb(II) and Hydrogel-I while solution pH determined the molecular interaction between the sorbate and adsorbent. Figure 11 displays that the effect of adsorbent dosage on the

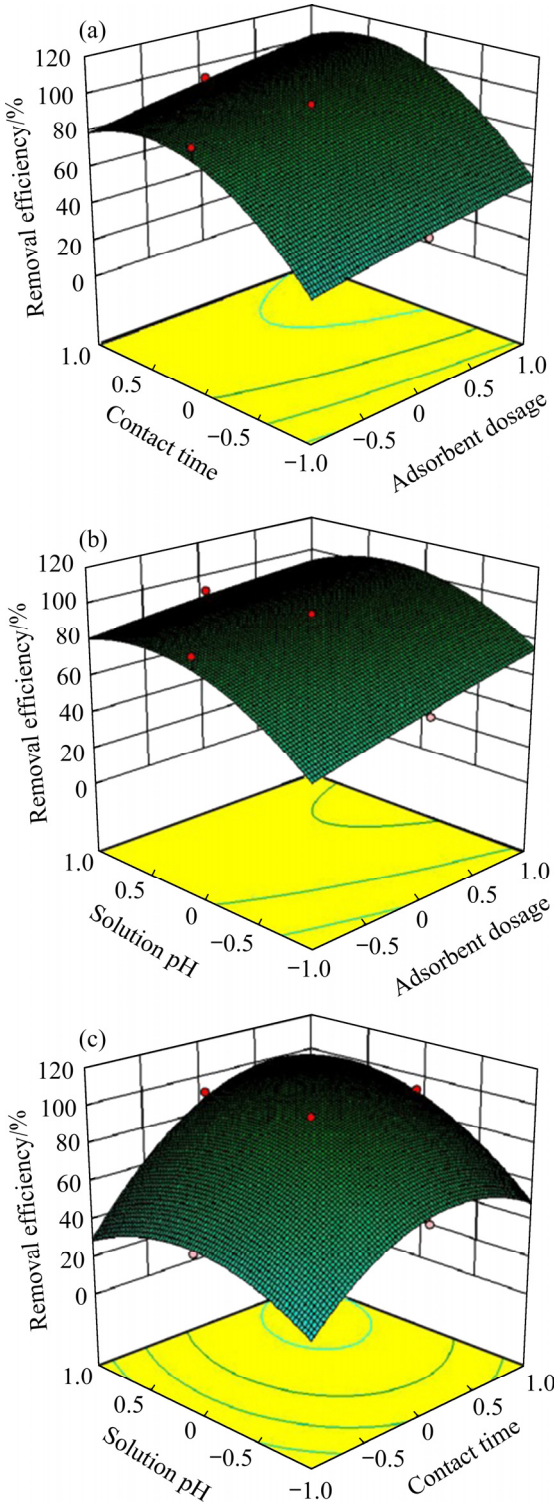

Fig. 10 Response surface plot showing interaction between contact time and adsorbent dosage (a), solution pH and adsorbent dosage (b), and solution pH and contact time (c)

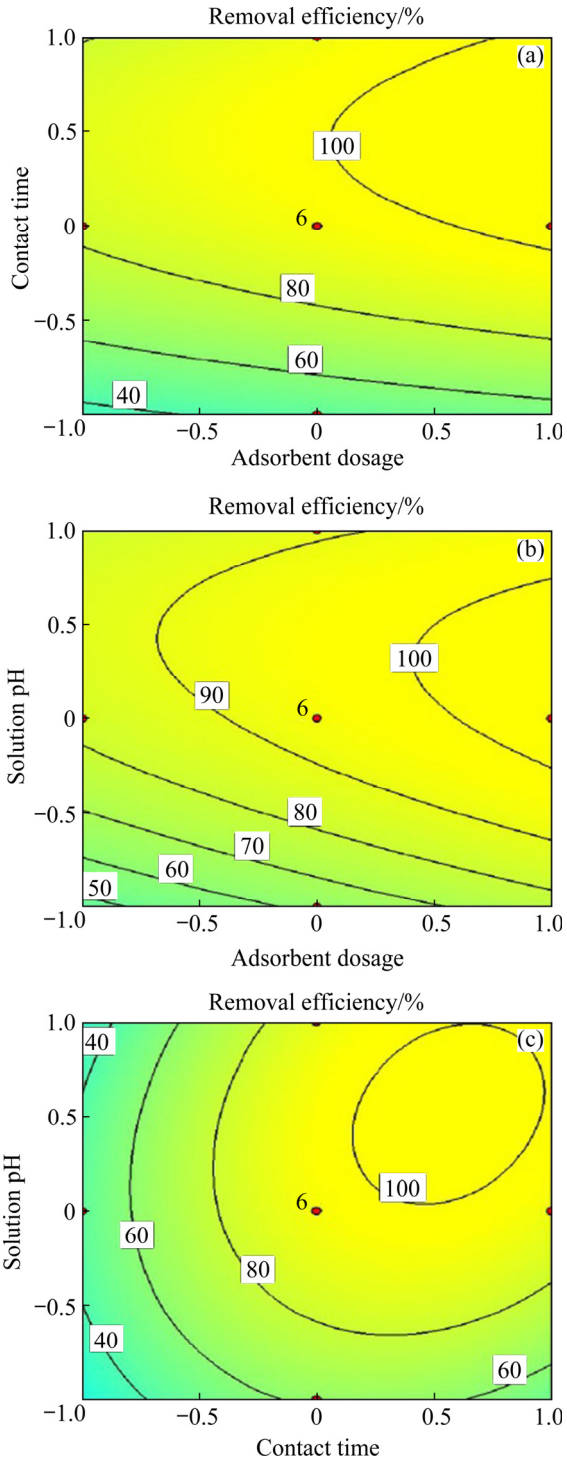

Fig. 11 Response surface interactive contour maps of contact time and adsorbent dosage (a), solution pH and adsorbent dosage (b), and solution pH and contact time (c)

adsorption efficiency of Pb(II) was smaller than that of contact time and solution pH, which might attribute to the fact that the adsorption active sites provided by Hydrogel-I were enough.

3.4 Adsorption mechanism

The uptake mechanism for Pb(II) over Hydrogel-I was speculated through the analysis of XPS spectra. According to the full scan survey mode (Fig. 12(a)), the existence of Pb was found

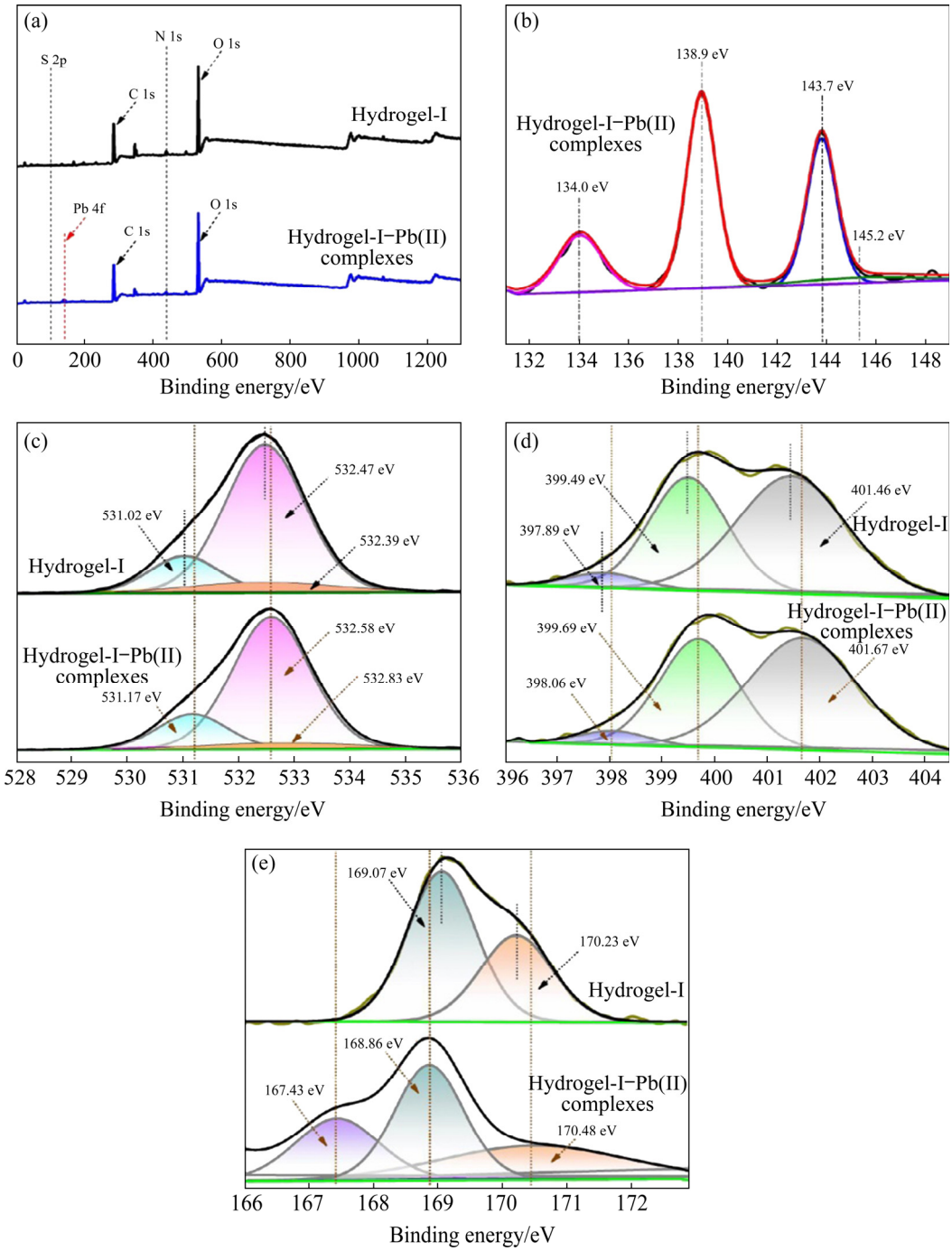

Fig. 12 Full scan survey XPS spectra (a) and high resolution spectra of Pb 4f (b), O 1s (c), N 1s (d) and S 2p (e)

in Hydrogel-I−Pb(II) complexes, proving the uptake of Pb(II) on the surface of Hydrogel-I. As displayed in Fig. 12(b), the peaks of Pb 4f were detected to be centered at 134.0, 138.9, 143.7 and 145.2 eV, in which the two peaks of 138.9 and 143.7 eV belonged to Pb $4f_{7/2}$ and Pb $4f_{5/2}$ [34], respectively. Compared to 139 eV and 143.9 eV in $Pb(NO_3)_2$ [34], these binding energies for Pb $4f_{7/2}$ and Pb $4f_{5/2}$ shifted towards negative direction (138.9 and 143.7 eV) accompanied with two peaks of 134.0 and 145.2 eV [34], suggesting that Pb—O was formed and inner-sphere complexation occurred [34]. According to Fig. 12(c), high-resolution spectra of O 1s for Hydrogel-I and Hydrogel-I−Pb(II) complexes, three peaks of O 1s emerging at 531.02, 532.39 and 532.47 eV in Hydrogel-I can be assigned to the groups of —OH, C═O and C—O—(C,H), respectively [23]. After

adsorption of Pb(II) over Hydrogel-I (Hydrogel-I−Pb(II) complexes) (Fig. 12(c)), the spectra of O 1s were shifted from 531.02, 532.39 and 532.47 eV to 531.17, 532.83 and 532.58 eV. These results demonstrated that the oxygen-containing functional groups carried by Hydrogel-I were involved in the removal of Pb(II), mainly including electrostatic attraction between —OH/—COO— and Pb(II) [35−37]. As seen from Fig. 12(d), three peaks for N 1s were discovered at 397.89, 399.49 and 401.46 eV corresponding to —NH, —NH_2 and C—N for Hydrogel-I [23]. After the adsorption of Pb(II) (Hydrogel-I−Pb(II) complexes), the peaks of 397.89 eV (—NH), 399.49 eV (—NH_2) and 401.46 (C—N) moved to 398.06, 399.69 and 401.67 eV (Fig. 12(d)), respectively, revealing that the nitrogen-containing functional groups carried by Hydrogel-I took part in the uptake of Pb(II), which may contain surface complexation since amine groups (—NH and —NH_2) reacted with Pb(II) through donating lone pair of nitrogen atom [38]. The high-resolution spectra of S 2p for Hydrogel-I and Hydrogel-I−Pb(II) complexes are exhibited in Fig. 12(e). As for Hydrogel-I, two peaks of 170.23 and 169.07 eV could be classified as C═S [25,26] and C—S [25,27], respectively. After the adsorption of Pb(II) (Hydrogel-I−Pb(II) complexes), the two peaks were observed to be shifted from 169.07 and 170.23 eV to 168.86 and 170.48 eV, respectively. Furthermore, one new peak at 167.43 eV due to the formation of S—Pb in Hydrogel-I−Pb(II) complexes [39] (Fig. 12(e)). These results suggested that the sulfur-containing functional groups of Hydrogel-I accounted for binding with Pb(II) such as electrostatic attraction between —CSS— and Pb(II) [40]. Furthermore, Fig. 8 presents pHpzc value of Hydrogel-I was determined to be 1.9, which suggested that deprotonation of the group could occur since solution pH was 6.0 in this work.

Based on the analyses of XPS spectra, the proposed mechanisms of Pb(II) adsorption over Hydrogel-I were presented as [36,40−43]

$$\equiv C—OH+Pb^{2+}\rightarrow\equiv C—O—Pb^{+}+H^{+} \quad (3)$$

$$2(\equiv C—OH)+Pb^{2+}\rightarrow(\equiv C—O)_2Pb^{+}+2H^{+} \quad (4)$$

$$R—COO—+Pb^{2+}\rightarrow(R—COO)_2Pb \quad (5)$$

$$\equiv C—NH+Pb^{2+}\rightarrow\equiv C—NH—Pb \quad (6)$$

$$\equiv C—NH_2+Pb^{2+}\rightarrow\equiv C—NH_2—Pb^{2+} \quad (7)$$

$$2(\equiv C—SS—)+Pb^{2+}\rightarrow(\equiv C—SS)_2—Pb \quad (8)$$

In summary, the functional groups containing —NH, —NH_2, —CSS— and —OH/—COOH on the surface of Hydrogel-I played different roles in the adsorption of Pb(II) via three types of combinations, as proposed in the following: (1) ions exchange of —OH and Pb(II), resulting in the formation of inner-sphere complexes (solution pH was measured and its value was reduced from initial 4.97 to final 3.57 (Fig. S7), confirming that H^+ was released during the adsorption of Pb(II)); (2) surface complexation between the amine groups of —NH/—NH_2 and Pb(II); (3) electrostatic attraction primarily between —CSS—/—COO— and Pb(II). Beyond these three interactions, the pore-filling effect was also considered to participate in the adsorption process of Pb(II) since the pore structures were discovered in Hydrogel-I by using SEM [44] (Fig. 3). The proposed adsorption mechanisms of Pb(II) over Hydrogel-I are displayed in Scheme 2.

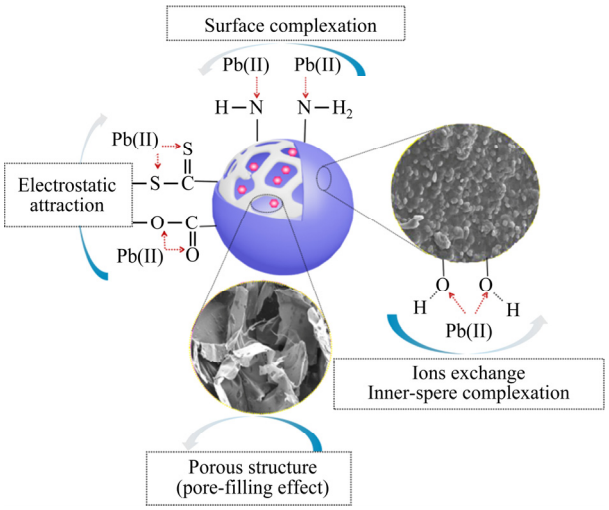

Scheme 2 Proposed removal mechanisms of Pb(II) over Hydrogel-I

3.5 Adsorption performance comparison

As mentioned above, Hydrogel-I was prepared via a mixture of MAL powders with SA. To compare the adsorption performance of Hydrogel-I with SA-$CaCl_2$ bead and MAL powders, the adsorption rate, adsorption amount and reusing ability were taken into account. The results and descriptions for adsorption kinetics, isotherms and thermodynamics are presented in Text S4 (SI). It was noted that the pseudo-second-order kinetic model could describe the experimental data well for Hydrogel-I, which was similar to MAL [9]. The

values of the rate constant (K_2) for Hydrogel-I were calculated to be 0.419 and 0.387 g/(mg·min) with C_0 of Pb(II) being 5 and 15 mg/L (Table S8), while for MAL they were obtained as 0.262 and 1.996 g/(mg·min) [9], respectively. The maximum adsorption capacities (q_m) of Pb(II) over Hydrogel-I, SA-$CaCl_2$ bead and MAL were 60.4 (Table 1), 10.0 (Table 1) and 79.9 mg/g [9], respectively. Figure 13(a) displays the residual concentration (C_r) of Pb(II) at different C_0 for Hydrogel-I. The value of C_r was measured as 0.05, 0.12 and 0.07 mg/L corresponding to C_0 of 1, 5 and 10 mg/L, meeting the discharged standard of 0.5 mg/L set by China for pollutants from inorganic chemical industry (GB 31573—2015) [45]. When C_0 was 15, 20 and 30 mg/L, C_r equaled 0.70, 0.68 and 0.98 mg/L, which all satisfied the integrated wastewater discharge standard of 1.0 mg/L from China (GB 8978—1996) [46]. Even under the situation of C_0=40 and 60 mg/L, C_r was discovered to be 1.89 and 2.20 mg/L, respectively (Fig. 13(a)). As for MAL (Fig. 13(b)), the value of C_r was measured to be 0.03, 0.20, 0.30, 0.75, 0.60 and 0.60 mg/L with C_0 value being 1, 5, 10, 15, 20 and 30 mg/L, respectively, which all complied with the emission standards of 1.0 mg/L (GB 8978 — 1996) [46]. These results demonstrated that the adsorption performance of Hydrogel-I towards Pb(II) was close to that of MAL. Moreover, the C_r of Pb(II) determined from SA−$CaCl_2$ bead corresponded to

Table 1 Parameters of isothermal models

Langmuir model			Freundlich model			DR model		
q_m/(mg·g^{-1})	K_L/(L·mg^{-1})	R^2	K_F/(mg·L$^{-(1-1/n)}$·g^{-1})	n	R^2	q_D/(mg·g^{-1})	E/(kJ·mol^{-1})	R^2
60.4	0.188	0.9859	1.701	0.196	0.9684	8.849	2.748	0.8624

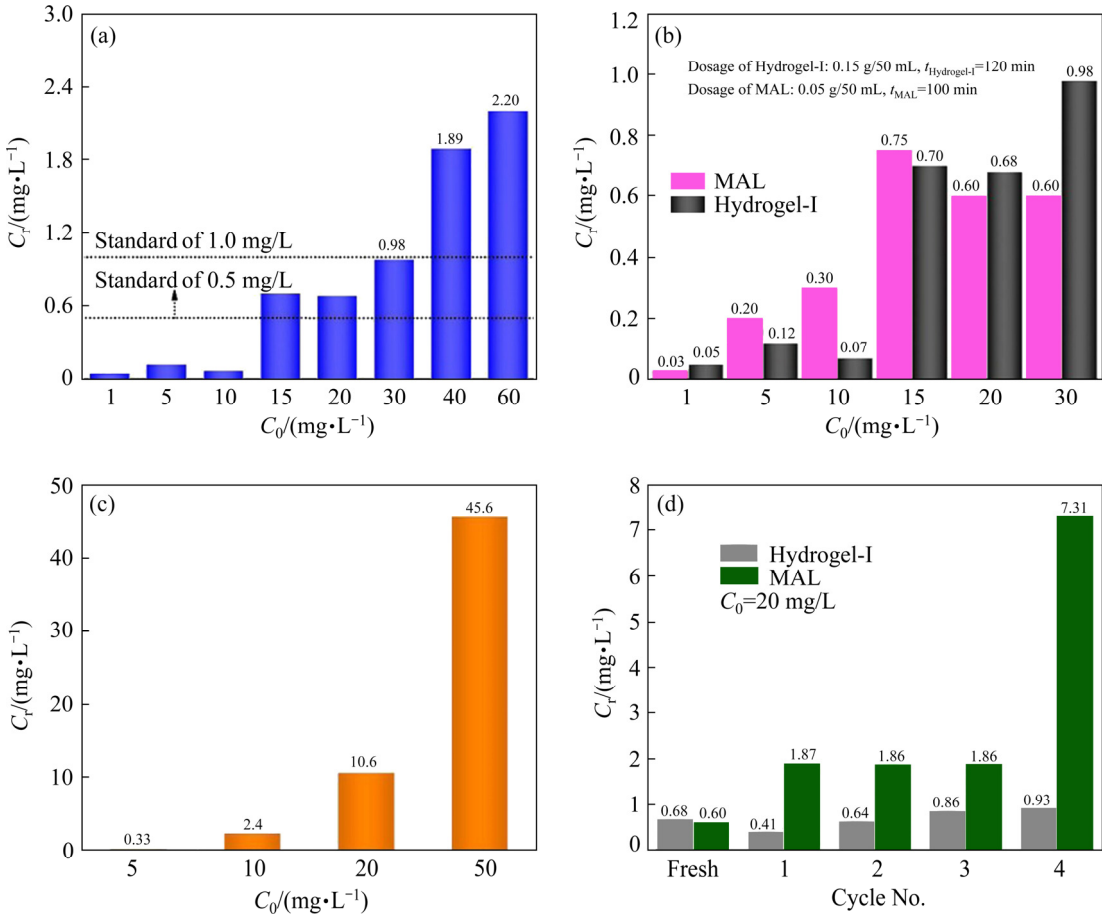

Fig. 13 Residual concentration (C_r) of Pb(II) over Hydrogel-I at contact time of 120 min (a); values of C_r for MAL and Hydrogel-I at C_0 of 1, 5, 10, 15, 20 and 30 mg/L (b); C_r of SA-$CaCl_2$ bead at C_0 of 5, 10, 20 and 50 mg/L (c); comparison of C_r between Hydrogel-I and MAL at each regeneration cycle (d)

Table 2 Comparison of Pb(II) adsorption between Hydrogel-I and pure MAL powder

Process		C_0/(mg·L^{-1})	C_r/(mg·L^{-1})		
			MAL	Hydrogel-I	Standard
Adsorption		1	0.03	0.05	0.5[a], 1.0[b]
		5	0.2	0.12	
		10	0.3	0.07	
		15	0.75	0.7	
		20	0.6	0.68	
		30	0.6	0.98	
Regeneration	Fresh	20	0.6	0.68	0.5[a], 1.0[b]
	Cycle 1		1.87	0.41	
	Cycle 2		1.86	0.64	
	Cycle 3		1.86	0.86	
	Cycle 4		7.31	0.93	

[a]– GB 31573—2015; [b]– GB 8978—1996

0.33, 2.4, 10.6 and 45.6 mg/L when C_0 was 5, 10, 20 and 50 mg/L (Fig. 13(c)), which showed that only 0.33 mg/L met the discharged standard of 0.5 mg/L (GB 31573 — 2015). These results suggested that SA−$CaCl_2$ bead possessed poor adsorption ability towards Pb(II).

In order to regenerate Hydrogel-I, HCl solution (0.2 mol/L) was selected as the stripping reagent to leach out Pb(II) adsorbed on the surface of Hydrogel-I. The values of C_r for fresh Hydrogel-I, regenerated Hydrogel-I for 1−4 cycles were 0.68, 0.41, 0.64, 0.86 and 0.93 mg/L (Fig. 13(d)), respectively. These values met with the integrated wastewater discharge standard of 1.0 mg/L regulated by China (GB 8978—1996). Under the same regenerating conditions, the values of C_r for MAL corresponded to 0.6, 1.87, 1.86, 1.86 and 7.31 mg/L (Fig. 13(d)). It can be concluded that Hydrogel-I has better regeneration ability than MAL. Table 2 gives the adsorption performance of Hydrogel-I and pure MAL powders.

Figure 14 shows that Hydrogel-I was more easily separated from solution than MAL powders after treatment. It can be seen that Hydrogel-I sunk to the bottom of beaker while MAL powders still suspended in aqueous solution after four adsorption−desorption cycles. The liquid color in the straw for MAL was brown, suggesting that MAL powders mixed with the effluent. However, liquid color in the straw for Hydrogel-I was transparent, further proving its better separability.

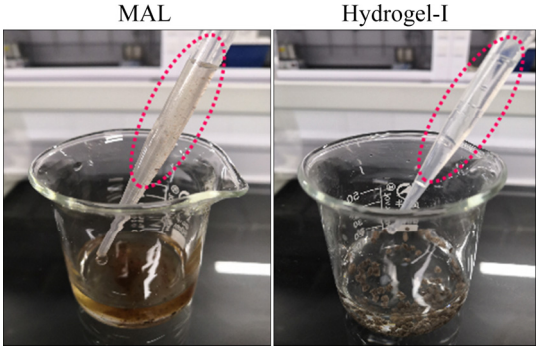

Fig. 14 Disperse and separation performance of MAL and Hydrogel-I

By comprehensively considering the adsorption rate, maximum adsorption capacity (q_m), regeneration ability and separation performance, the application potential of Hydrogel-I was better than that of MAL.

Adsorption performances of Hydrogel-I towards Pb(II) were compared to other kinds of organic hydrogel adsorbents (Table 3) based on the viewpoints of adsorption capacity, adsorption rate and equilibrium time. The value of K_2 for Hydrogel-I was 0.387 g/(mg·min) as C_0 of Pb(II) was 15 mg/L. At similar C_0 level, K_2 values of adsorbents I, II, III, V, VIII, IX, X, XII and XIII were correspondingly 0.038, 0.0002, 0.015, 0.019, 0.049, 0.0008, 0.006, 0.043 and 0.038 g/(mg·min), obviously lower than that of Hydrogel-I. As for adsorbents IV and XI, the C_0 values were set at 48 and 65 mg/L, respectively, several times higher than

Table 3 Comparison of adsorption performance among Hydrogel-I and other kinds of hydrogel adsorbents

Adsorbent	C_0/ (mg·L^{-1})	K_2/ (g·mg^{-1}·min^{-1})	Equilibrium time/min	pH	q_m/ (mg·g^{-1})	Ref.
SA−$CaCl_2$ bead	15	0.0132	120	6.0	10.0	This work
Hydrogel-I	15	0.387	120	6.0	60.4	This work
WSC−g-PKA/PVA (I)	25	0.038	120	6.0	112	[47]
Magnetic bio-sorbent hydrogel (II)	20	0.0002	1440	5.0	81.8	[48]
MBCG (III)	20	0.015	4320	*n*	70.9	[49]
XCMCP (IV)	48	0.006	1440	6.8	59.9	[50]
CTPP (IPN) hydrogels (V)	10	0.019	100	4.5	57.3	[51]
Cellulose−MT-CBM (VI)	−	−	60	6.5	39	[52]
ATP/P(AA-co-AM) (VII)	−	−	960	5.0	35.9	[53]
WT-g-AA (VIII)	10	0.049	120	7.0	35.7	[54]
P123-DA (IX)	3	0.0008	720	7.0	35.2	[55]
Poly(acrylic acid)/nanosorbent (X)	20	0.006	1140	6.0	33.3	[56]
OPB/PVA/MWCNTs (XI)	65	0.005	120	6.0	29.5	[57]
FLSG (XII)	10	0.043	120	5.5	19.6	[58]
TLSG (XIII)	10	0.038	120	5.5	17.9	[58]

I: Wheat straw cellulose−g-poly (potassium acrylate)/polyvinyl alcohol; III: MnO_2 modified biochar-based porous hydrogel; IV: Xanthate-modified cross-linked magnetic chitosan/poly(vinyl alcohol); V: Chitosan−tripolyphosphate beads; VI: Metallothionein/ cellulose; VII: Covalently crosslinked attapulgite/poly(acrylic acid-co-acrylamide) nanocomposite hydrogel; VIII: Acrylic acid-grafted waste textiles; IX: Di-acrylated Pluronic P123 hydrogels; XI: Oil palm bio-waste/MWCNTs reinforced PVA hydrogel composites; XII: 2-furoyl loaded silica gel; XIII: 2-thiophenecarbonyl loaded silica gel

that of Hydrogel-I. It is generally believed that higher C_0 would enhance the adsorption driving force. However, the K_2 values for adsorbents IV and XI were as low as 0.006 and 0.005 g/(mg·min), respectively. As presented in Table 3, the value of q_m for Hydrogel-I was 60.4 mg/g, demonstrating an advantage of Pb(II) uptake over adsorbents IV−XIII. It was observed that q_m value of adsorbents I−III was higher than that of Hydrogel-I while their equilibrium time was longer. By considering adsorption rate, adsorption amount and equilibrium time, it can be concluded that Hydrogel-I possesses better adsorption performance.

4 Conclusions

(1) The synthesized conditions for Hydrogel-I were optimized, in which initiator (SA) composition was 1.20 wt.%, crosslinker concentration ($CaCl_2$) was 0.23 mol/L and MAL powder amount was 0.3400 g. The physical-chemical properties of Hydrogel-I were characterized, including morphology, chemical composition, thermostability and compressive performance.

(2) When Pb(II) was selected as the target pollutant, the optimal operating conditions were determined to be Hydrogel-I dosage of 3.0 g/L, contact time of 13 min and solution pH of 6.0. Analysis on adsorption mechanism revealed that ions exchange, surface complexation, electrostatic attraction and pore-filling effect may contribute to the adsorption of Pb(II) onto Hydrogel-I. The functional groups of —NH, —NH_2, —CSS—, —OH and —COO— were responsible for binding with Pb(II).

(3) The adsorption performance of Hydrogel-I towards Pb(II) was compared with that of MAL powders. It was indicated that adsorption rate and the maximum adsorption capacity (q_m) of the two adsorbents were close while the regeneration ability and separation from aqueous solution of Hydrogel-I were better than those of MAL powders. Even compared with organic hydrogel materials, Hydrogel-I presented quicker adsorption and higher adsorption capacity, showing that Hydrogel-I possesses a promising application potential for treatment of Pb(II)-loaded wastewater.

Acknowledgments

This work was funded by the National Key Research and Development Project (No. 2019YFC1804800), Key R&D Program of Shaanxi Province, China (No. 2019SF-253), the

Fundamental Research Funds for the Central Universities, China (No. 300102291504), the Pearl River S&T Nova Program of Guangzhou, China (No. 201710010065), the Science and Technology Program of Guangdong Forestry Administration, China (No. 2020-KYXM-08), and the Key Laboratory of Resource Chemistry, Ministry of Education, China (No. KLRC_ME2102). We are very thankful for the support of the Instrument Analysis Center of Xi'an Jiaotong University, China.

Supporting information

The Supporting information can be found at: http://www.ysxbcn.com/download/25-p2770-2021-0770-supporting-materials.pdf

References

[1] ZHU Zeng-li, LIU Huan, CHEN Jie-shuang-yang, KONG Hui, XU Liang, HUA Zhong-sheng, ZHAO Zhuo. Electrochemical behavior and electrolytic preparation of lead in eutectic NaCl−KCl melts [J]. Transactions of Nonferrous Metals Society of China, 2020, 30: 2568−2576.

[2] DU Jiao, SHANG Xiao-xian, LI Tao, GUAN Yue-ping. Recycling and modeling of chromium from sludge produced from magnetic flocculation treatment of chromium-containing wastewater [J]. Process Safety and Environmental Protection, 2022, 157: 1−7.

[3] SUN Meng, QIN Mo-han, WANG Chi, WENG Guo-ming, HUO Ming-xin, TAYLOR A D, QU Jiu-hui, ELIMELECH M. Electrochemical-osmotic process for simultaneous recovery of electric energy, water, and metals from wastewater [J]. Environmental Science and Technology, 2020, 54: 8430−8442.

[4] LU Min, ZHANG Yue-ming, GUAN Xiao-hui, XU Xiao-hui, GAO Ting-ting. Thermodynamics and kinetics of adsorption for heavy metal ions from aqueous solutions onto surface amino-bacterial cellulose [J]. Transactions of Nonferrous Metals Society of China, 2014, 24: 19127−1917.

[5] GOMES P I A, ASAEDA T. Phytoremediation of heavy metals by calcifying macro-algae (*Nitella pseudoflabellata*): Implications of redox insensitive end products [J]. Chemosphere, 2013, 92: 1328−1334.

[6] CAO Xin-de, MA Le-na, LIANG Yuan, GAO Bin, HARRIS W. Simultaneous immobilization of lead and atrazine in contaminated soils using dairy-manure biochar [J]. Environmental Science and Technology, 2011, 45: 4884−4889.

[7] ADHIKARI B B, GURUNG M, ALAM S, TOLMAI B, INOUE K. Kraft mill lignin—A potential source of bio-adsorbents for gold recovery from acidic chloride solution [J]. Chemical Engineering Journal, 2013, 231: 190−197.

[8] ALBADARIN A B, AL-MUHTASEB A H, AL-LAQTAH N A, WALKER G M, ALLEN S J, AHMAD M N M. Biosorption of toxic chromium from aqueous phase by lignin: Mechanism, effect of other metal ions and salts [J]. Chemical Engineering Journal, 2011, 169: 1−3.

[9] WANG Qiao-rui, ZHENG Chun-li, SHEN Zhen-xing, LU Qiang, HE Chi, ZHANG T C, LIU Jian-hui. Polyethyleneimine and carbon disulfide co-modified alkaline lignin for removal of Pb^{2+} ions from water [J]. Chemical Engineering Journal, 2019, 359: 265−274.

[10] DEMIRBAS A. Adsorption of lead and cadmium ions in aqueous solutions onto modified lignin from alkali glycerol delignication [J]. Journal of Hazardous Materials, 2004, 109: 221−226.

[11] MELO D Q, NETO V O S, OLIVEIRA J T, BARROS A L, GOMES E C C, RAULINO G S C, LONGUINOTTI E, NASCIMENTO R F. Adsorption equilibria of Pb^{2+}, Zn^{2+}, and Cd^{2+} on EDTA-functionalized silica spheres [J]. Journal of Chemical and Engineering Data, 2013, 58: 798−806.

[12] REN Hui-xue, GAO Zhi-min, WU Dao-ji, JIANG Jia-hui, SUN You-min, LUO Cong-wei. Efficient Pb(II) removal using sodium alginate-carboxymethyl cellulose gel beads: Preparation, characterization, and adsorption mechanism [J]. Carbohydrate Polymers, 2016, 137: 402−409.

[13] SHAN Su-jie, TANG Huan, ZHAO Ying, WANG Wei, CUI Fu-yi. Highly porous zirconium-crosslinked graphene oxide/alginate aerogel beads for enhanced phosphate removal [J]. Chemical Engineering Journal, 2019, 359: 779−789.

[14] JIANG Hua-bin, YANG Yu-ru, LIN Zong-kun, ZHAO Bin-chan, WANG Jing, XIE Jun, ZHANG Ai-ping. Preparation of a novel bio-adsorbent of sodium alginate grafted polyacrylamide/graphene oxide hydrogel for the adsorption of heavy metal ion [J]. Science of the Total Environment, 2020, 744: 140653.

[15] HU Zhao-Hong, OMER A M, OUYANG Xiao-kun, YU Di. Fabrication of carboxylated cellulose nanocrystal/sodium alginate hydrogel beads for adsorption of Pb(II) from aqueous solution [J]. International Journal of Biological Macromolecules, 2018, 108: 149−157.

[16] ZHANG Hong, OMER A M, HU Zhao-hong, YANG Li-Ye, JI Chao, OUYANG Xiao-kun. Fabrication of magnetic bentonite/carboxymethyl chitosan/sodium alginate hydrogel beads for Cu(II) adsorption [J]. International Journal of Biological Macromolecules, 2019, 135: 490−500.

[17] PERETZ S, ANGHEL D F, VASILESCU E, FLOEA-SPIROIU M, STOIAN C, ZGHEREA G. Synthesis, characterization and adsorption properties of alginate porous beads [J]. Polymer Bulletin, 2015, 72: 3169−3182.

[18] CELIK E, BAYRAM C, AKCAPINAR R, TYRK M, DENKBAS E B. The effect of calcium chloride concentration on alginate/Fmoc-diphenylalanine hydrogel networks [J]. Materials Science and Engineering C−Materials for Biological Applications, 2016, 66: 221−229.

[19] WANG Min, LI Xiong, ZHANG Tong-hui, DENG Li, LI Pei-yun, WANG Xue-fen, HSIAO B S. Eco-friendly poly(acrylic acid)-sodium alginate nanofbrous hydrogel: A multifunctional platform for superior removal of Pb(II) and sustainable catalytic applications [J]. Colloids and Surfaces, A: Physicochemical and Engineering Aspects, 2018, 558: 228−241.

[20] WANG Min, LI Xiong, HUA Wei-kang, SHEN Ling-di, YU Xu-feng, WANG Xue-fen. Electrospun poly(acrylic

acid)/silica hydrogel nanofibers scaffold for highly efficient adsorption of lanthanide ions and its photoluminescence performance [J]. ACS Applied Materials and Interfaces, 2016, 8: 23995−24007.

[21] FAN Jin-chen, SHI Zi-xing, LIAN Min, LI Hong, YIN Jie. Mechanically strong graphene oxide/sodium alginate/ polyacrylamide nanocomposite hydrogel with improved dye adsorption capacity [J]. Journal of Materials Chemistry A, 2013, 1: 7433−7443.

[22] THAKUR P S, PANDEY S, AROTIBA O A. Development of a sodium alginate-based organic/inorganic superabsorbent composite hydrogel for adsorption of methylene blue [J]. Carbohydrate Polymers, 2016, 153: 34−46.

[23] WU Hong-ye, GONG Lang, ZHANG Xin, HE Fu-ren, LI Zhi-li. Bifunctional porous polyethyleneimine-grafted lignin microspheres for efficient adsorption of 2,4-dichlorophenoxyacetic acid over a wide pH range and controlled release [J]. Chemical Engineering Journal, 2021, 411: 128539.

[24] LIU Li-hua, WU Jun, LI Xin, LING Yu-lin. Synthesis of poly(dimethyldiallylammonium chloride-co-acrylamide)-graft-triethylenetetramine-dithiocarbamate and its removal performance and mechanism of action towards heavy metal ions [J]. Separation and Purification Technology, 2013, 103: 92−100.

[25] YANG Zheng-chi, LIU Li-hua, LIU Si-yan, SU Gang, LIU Xing, TANG An-ping, XUE Jian-rong, ZENG Meng-xiang. Synthesis of dithiocarbamate-modified crosslinked poly (β-cyclodextrin-cotriethylenetetramine) microspheres for simultaneous and highly efficient removal of Cu^{2+} and methyl orange/thymol blue from wastewater [J]. Reactive and Functional Polymers, 2021, 159: 104809.

[26] CHEN Yun-long, ZI Fu-ting, HU Xian-zhi, YU Hong, NIE Yan-he, YANG Peng, CHENG Hui-ling, WANG Qiang, QIN Xue-cong, CHEN Shu-liang, ZHANG Yan. Grafting of organic sulfur-containing functional groups on activated carbon for gold(I) adsorption from thiosulfate solution [J]. Hydrometallurgy, 2019, 185: 102−110.

[27] SAHA D, BARAKAT S, VAN-BRAMER S E, NELSON K A, HENSLEY D K, CHEN J. Noncompetitive and competitive adsorption of heavy metals in sulfur-functionalized ordered mesoporous carbon [J]. ACS Applied Materials and Interfaces, 2016, 8: 34132−34142.

[28] SHAO Zi-jian, HUANG Xue-lian, YANG Fan, ZHAO Wei-feng, ZHOU Xin-zhi, ZHAO Chang-sheng. Engineering sodium alginate-based cross-linked beads with high removal ability of toxic metal ions and cationic dyes [J]. Carbohydrate Polymers, 2018, 187: 85−93.

[29] TALEB F, AMMAR M, MOSBAH M B, SALEM R B, MOUSSAOUI Y. Chemical modifcation of lignin derived from spent cofee grounds for methylene blue adsorption [J]. Scientific Reports, 2020, 10: 11048.

[30] THAKUR S, AROTIBA O A. Synthesis, swelling and adsorption studies of a pH responsive sodium alginate-poly(acrylic acid) superabsorbent hydrogel [J]. Polymer Bulletin, 2018, 75: 4587−4606.

[31] YUE Yi-ying, WANG Xian-hui, HAN Jing-quan, YU Lei, CHEN Jian-qiang, WU Qing-lin, JIANG Jian-chun. Effects of nanocellulose on sodium alginate/polyacrylamide hydrogel: Mechanical properties and adsorption−desorption capacities [J]. Carbohydrate Polymers, 2019, 206: 289−301.

[32] LI Hui, MENG Hua, YANG Yan-Yu, HUANG Jia-Xi, CHEN Yong-Jie, YANG Fei, YAN Jia-Zhi. A double-network hydrogel for the dynamic compression of the lumbar nerve root [J]. Neural Regeneration Research, 2020, 15: 1724−1731.

[33] ZHAO Wei-wei, SHI Zhi-jun, CHEN Xiu-li, YANG Guang, LENARDI C, LIU Chang-qing. Microstructural and mechanical characteristics of PHEMA-based nanofibre-reinforced hydrogel under compression [J]. Composites, Part B: Engineering, 2015, 76: 292−299.

[34] ZHANG Bao-lin, QIU Wei, WANG Pan-pan, LIU Yu-lei, ZOU Jing, WANG Lu, MA Jun. Mechanism study about the adsorption of Pb(II) and Cd(II) with irontrimesic metal−organic frameworks [J]. Chemical Engineering Journal, 2020, 385: 123507.

[35] FU Weng, HUANG Zhi-qiang. Magnetic dithiocarbamate functionalized reduced graphene oxide for the removal of Cu(II), Cd(II), Pb(II), and Hg(II) ions from aqueous solution: Synthesis, adsorption, and regeneration [J]. Chemosphere, 2018, 209: 449−456.

[36] ZHU Qian, LI Zheng-kui. Hydrogel-supported nanosized hydrous manganese dioxide: Synthesis, characterization, and adsorption behavior study for Pb^{2+}, Cu^{2+}, Cd^{2+} and Ni^{2+} removal from water [J]. Chemical Engineering Journal, 2015, 281: 69−80.

[37] ZHAO Han, OUYANG Xiao-kun, YANG Li-ye. Adsorption of lead ions from aqueous solutions by porous cellulose nanofiber-sodium alginate hydrogel beads [J]. Journal of Molecular Liquids, 2021, 324: 115122.

[38] LIU Yan, GAO Qiang, LI Chen, LIU Shu, XIA Kai-sheng, HAN Bo, ZHOU Cheng-gang. Effective coating of crosslinked polyethyleneimine on elastic spongy monolith for highly efficient batch and continuous flow adsorption of Pb(II) and acidic red 18 [J]. Chemical Engineering Journal, 2020, 391: 123610.

[39] ZHU Ye-hua, HU Jun, WANG Jian-long. Competitive adsorption of Pb(II), Cu(II) and Zn(II) onto xanthate-modified magnetic chitosan [J]. Journal of Hazardous Materials, 2012, 221: 155−161.

[40] IFTHIKAR J, SHAHIB I I, SELLAOUI L, JAWAD A, ZHAO M M, CHEN Z Q, CHEN Z L. pH tunable anionic and cationic heavy metal reduction coupled adsorption by thiol cross-linked composite: Physicochemical interpretations and fixed bed column mathematical model study [J]. Chemical Engineering Journal, 2019, 401: 126041.

[41] HUA Rong, LI Zheng-kui. Sulfhydryl functionalized hydrogel with magnetism: Synthesis, characterization, and adsorption behavior study for heavy metal removal [J]. Chemical Engineering Journal, 2014, 249: 189−200.

[42] XU Xin-yi, OUYANG Xiao-kun, YANG Li-Ye. Adsorption of Pb(II) from aqueous solutions using crosslinked carboxylated chitosan/carboxylated nanocellulose hydrogel beads [J]. Journal of Molecular Liquids, 2021, 322: 114523.

[43] ZHAO Han, OUYANG Xiao-Kun, YANG Li-Ye. Adsorption of lead ions from aqueous solutions by porous cellulose nanofiber-sodium alginate hydrogel beads [J]. Journal of Molecular Liquids, 2021, 324: 115122.

[44] ZHANG Wei, SONG Jian-yang, HE Qiu-lai, WANG Hong-yu, LYU Wan-lin, FENG Hui-juan, XIONG Wen-qi, GUO Wen-bin, WU Jing, CHEN Ling. Novel pectin based

composite hydrogel derived from grapefruit peel for enhanced Cu(II) removal [J]. Journal of Molecular Liquids, 2020, 384: 121445.
[45] GB 31573—2015. Emission standards of pollutants for inorganic chemical industry [S]. 2015.
[46] GB 8978—1996. Integrated wastewater discharge standard [S]. 1996.
[47] SU Yuan, LIU Jia, YUE Qin-yan, LI Qian, GAO Bao-yu. Adsorption of lead and nickel ions by semi-interpenetrating network hydrogel based on wheat straw cellulose: Kinetics, Equilibrium, and Thermodynamics [J]. Soft Materials, 2015, 13: 225−236.
[48] SAHRAEI R, POUR Z S, GHAEMY M. Novel magnetic bio-sorbent hydrogel beads based on modified gum tragacanth/graphene oxide: Removal of heavy metals and dyes from water [J]. Journal of Cleaner Production, 2017, 142: 2973−2984.
[49] WU Zhi-ying, CHEN Xiao-xiao, YUAN Bao-ling, FU Ming-Lai. A facile foaming-polymerization strategy to prepare 3D MnO_2 modified biochar-based porous hydrogels for efficient removal of Cd(II) and Pb(II) [J]. Chemosphere, 2020, 239: 124745.
[50] LV Long, CHEN Nan, FENG Chuan-ping, ZHANG Jing, LI Miao. Heavy metal ions removal from aqueous solution by xanthate-modified cross-linked magnetic chitosan/poly(vinyl alcohol) particles [J]. RSC Advances, 2017, 7: 27992−28000.
[51] NGAH W S W, FATINATHAN S. Adsorption characterization of Pb(II) and Cu(II) ions onto chitosan-tripolyphosphate beads: Kinetic, equilibrium and thermodynamic studies [J]. Journal of Environmental Management, 2010, 91: 958−969.
[52] MWANDIRA W, NAKASHIMA K, TOGO Y, SATO T, KAWASAKI S. Cellulose-metallothionein biosorbent for removal of Pb(II) and Zn(II) from polluted water [J]. Chemosphere, 2020, 246: 125733.
[53] LIU Peng, JIANG Li-ping, ZHU Long-xiang, GUO Jin-shan, WANG Ai-qin. Synthesis of covalently crosslinked attapulgite/poly(acrylic acid-co-acrylamide) nanocomposite hydrogels and their evaluation as adsorbent for heavy metal ions [J]. Journal of Industrial and Engineering Chemistry, 2015, 23: 188−193.
[54] ZHOU Tao, XIA Fa-fa, DENG Yue, ZHAO You-cai. Removal of Pb(II) from aqueous solutions using waste textiles/poly(acrylic acid) composite synthesized by radical polymerization technique [J]. Journal of Environmental Sciences, 2018, 67: 368−377.
[55] SHEN Chong, PENG Bin, WANG Ying, MENG Qin. Pb^{2+} and Hg^{2+} removal from polluted milk by di-acrylated Pluronic P123 hydrogels [J]. Food Chemistry, 2018, 258: 331−336.
[56] BHATIA M, RAJULAPATI S B, SONAWANE S, GIRDHAR A. Synthesis and implication of novel poly(acrylic acid)/nanosorbent embedded hydrogel composite for lead ion removal [J]. Scientific Reports, 2017, 7: 16413.
[57] ZULFIAAR M, LEE S Y, MAFIZE A A, KAHAR N A M A, JOHARI K, RABAT N E. Efficient removal of Pb(II) from aqueous solutions by using oil palm bio-waste/MWCNTs reinforced PVA hydrogel composites: Kinetic, isotherm and thermodynamic modeling [J]. Polymers, 2020, 12: 430.
[58] KUSHWAHA A K, GUPTA N, CHATTOPADHYAYA M C. Adsorption behavior of lead onto a new class of functionalized silica gel [J]. Arabian Journal of Chemistry, 2017, 10: s81−s89.

一种 MAL 改性水凝胶球珠对铅离子的吸附

郑春莉[1,2]，王巧蕊[1]，耿国庆[3]，王振兴[4]，卓 恒[5]

1. 西安交通大学 环境科学与工程系，西安 710049；
2. 长安大学 旱区地下水文与生态效应教育部重点实验室，西安 710049；
3. Department of Civil and Environmental Engineering, National University of Singapore, 117576, Singapore；
4. 生态环境部华南环境科学研究所，广州 510655；
5. 江苏泰斯特专业检测有限公司，宿迁 223800

摘 要：采用海藻酸钠对 MAL 粉末进行包埋制备水凝胶材料 Hydrogel-I，并将其应用于水中铅离子的去除。采用响应曲面法结合中心复合设计优化 Hydrogel-I 的制备条件及其吸附 Pb(II)的操作条件。XPS 揭示 Hydrogel-I 携带的—OH、—COO—、—NH、—NH_2 和—CSS 等官能团与 Pb(II)产生吸附结合。在吸附过程中，离子交换、表面络合、静电吸引和孔填充均发挥作用。比较 Hydrogel-I 凝胶颗粒和 MAL 粉末对 Pb(II)的吸附性能。虽然上述两种材料具有较为接近的吸附速率和最大吸附量(q_m)，但 Hydrogel-I 表现出更好的重复利用性，同时，更容易从水溶液中分离出来。与其他有机水凝胶材料相比，Hydrogel-I 具有较快的吸附速度和较高的吸附容量。上述结果表明，Hydrogel-I 具备较好应用潜能，可用于 Pb(II)的吸附。

关键词：吸附；MAL 粉末；水凝胶颗粒；Pb(II)

(Edited by Bing YANG)